# Defect-Engineered ZnO/BTO Photoanodes for Enhanced Solar-driven Photoelectrochemical Desalination of High-Salinity Coal Chemical Wastewater

Jianrong Li[a], Min Luo [a, *], Yipeng Zhao [a], Shengbo Yuan [a], Yongqing Yang [a], Xiaoman Li [a, *], Kwan San Hui [b], Fuming Chen [c, *]

[a] State Key Laboratory of High-efficiency Utilization of Coal and Green Chemical Engineering, School of Chemistry and Chemical Engineering, Ningxia University, Yinchuan, Ningxia 750021, P. R. China

[b] Department of Mechanical Engineering, College of Engineering, Prince Mohammad Bin Fahd University, P.O. Box 1664, Al Khobar 31952, Kingdom of Saudi Arabia

[c] State Key Laboratory of Tropic Ocean Engineering Materials and Materials Evaluation, School of Chemistry and Chemical Engineering, Hainan University, Haikou, Hainan 570228, P. R. China

# Contents

## S1. Additional experimental details

### S1.1 Photoanode-Assisted Electrochemical Desalination (PA-ED) Device

The PA-ED device contains two redox streams and two salt streams separated by ion-exchange membranes. The redox electrolyte was circulated using a peristaltic pump. The salt feed (NaCl solution or real high-salinity wastewater, 10 mL) was circulated in the salt channels, and the salt concentration was monitored using a conductivity meter. The active area of each electrode plate was 1 $cm^2$ and the device thickness was 4 mm. The chambers and conductivity-detection cells were made of polytetrafluoroethylene (PTFE) and equipped with inlet/outlet ports for capillaries.

Redox electrolyte: a mixture of 0.03 M $I_2$ and 1.0 M NaI with an additive (as prepared in the experiments) in a total volume of 10 mL. The flow rate is controlled at 1 mL/min using a soft tube with an inner diameter of 1.5 mm.

### S1.2 Solar-driven desalination evaluation

Desalination performance was evaluated using a photoelectrochemical system under zero-bias conditions. A xenon lamp (CEAULIGHT CEL-S500) was served as the light source, with incident irradiance quantified by a UV-365 solar radiometer (Beijing Shida Photoelectric Technology). Electrochemical measurements, including chronoamperometry (CA) and constant-current discharge profiles, were conducted on a DH7003 workstation (DONGHUA). The flow rates in both salt and redox chambers are maintained at 5 mL/min using a peristaltic pump (Kamoer NP04-KCS-B146). The conductivity of the salt solution was monitored in real time using a DDSJ-308F conductivity meter.

The salt removal rate (SRR, μg/($cm^2$·min)) represents the desalination ability of PEC desalination per time unit and active region, which can be calculated using the below equation:

$$SRR = \frac{\frac{\Delta c}{\Delta t} \times V}{A_{Cell}} \quad (1)$$

Where $\frac{\Delta c}{\Delta t}$ represents the salt concentration change per minute (mg/(L·min)), V is the total volume of one salt chamber (mL), and $A_{cell}$ represents the active area of the PEC desalination device ($cm^2$).

The solar desalination capacity (Ec, μmol/J) is calculated as follows:

$$Ec = \frac{\Delta c \times V \times 10^6}{P \times \Delta t \times A_{Cell}} \quad (2)$$

### S1.3 Photoelectrochemical measurements and calculations

The electrochemical cyclic voltammetry (CV) was performed on a workstation (CHI660D). The measurement of I-V curve, Mott-Schottky, open-circuit voltage (OCP-t) and EIS were measured using an electrochemical workstation (CHI760E). A standard three-electrode system was employed, consisting of a photoanode as working electrode, an Ag/AgCl as reference electrode and a Pt sheet as counter electrode, as well as a 0.1 M $K_2SO_4$ as electrolyte solution(pH=7).

The key equations used in analysis are listed as follows:

$$\tau = -\frac{\kappa_B T}{e}\left(\frac{dOCP}{dt}\right)^{-1} \quad (3)$$

where τ represents the lifetime of photogenerated carriers, $k_B$ represents thermal energy ($1.38\times10^{-23}$ $J\cdot K^{-1}$), e represents the charge power ($1.602\times10^{-19}$ C), and T represents thermodynamic temperature (293.15 K).

$$(\alpha h\nu)^{1/n}=A(h\nu-Eg) \quad (4)$$

Where the parameters of the Tauc equation are defined as follows: α (absorption coefficient), hν (photon energy), A (absorbance), and Eg (bandgap energy). The exponent n takes values of 1/2 and 2, corresponding to direct bandgap and indirect bandgap semiconductors, respectively.

$$E_{VB,NHE}=\varphi+E_{VB,XPS}-0.44 \quad (\varphi=2.20\ eV) \quad (5)$$

Where $E_{VB}$ and φ represent the valence band potential of the semiconductor and the work function of the instrument, respectively.

$$(E_{VB}=E_{CB}-Eg) \quad (6)$$

Where $E_{VB}$, $E_{CB}$ and Eg are defined as the valence band potential, conduction band potential, and band gap of the semiconductor, respectively.

$$E_{F,redox}=-4.5eV-e_0E_{redox} \quad (7)$$

Among them, $E_{redox}$ and $E_{F,redox}$ are the redox potential and the Fermi level of the redox species respectively, and eo = 1 (electron). According to equation (7), $E_{F,redox}$ was measured to be -5.25 eV, which is lower than the valence band position of ZnO. From a thermodynamic perspective, the redox species in the electrolyte can inject holes into the valence band of the photoanode, thereby driving the redox reaction.

**S1.4 Characterization**

Structural and compositional characterization was systematically performed using multi-technique analysis. Phase identification was measured by using a Bruker D8 ADVANCE A25 XRD system (Cu Kα radiation). Raman spectroscopy was conducted on a LabRam HR Evolution spectrometer with 455 nm laser excitation. Microstructural analysis was performed using, (1) a Thermo Scientific Quattro S field-emission SEM equipped with EDAX ELECT P; (2) a FEI Talos F200X TEM with energy-dispersive X-ray spectroscopy (EDX) system. Surface chemistry was investigated by using X-ray photoelectron spectroscopy (XPS, USA, Thermo Scientific K-Alpha). In-situ irradiation XPS (SI-XPS) spectra were obtained on the ESCALAB 250Xi (Thermo Fischer, USA) X-ray photoelectron spectrometer. The Fourier transform infrared (FT-IR) spectra were acquired using a Nicolet iN10 micro-FTIR spectrometer (Thermo Scientific, USA) with KBr pellets (1:100 sample/KBr ratio), Optoelectronic properties were evaluated by UV-vis diffuse reflectance spectra (UV-vis DRS) (TU-1900, Pu-Analysis Inc). Electron paramagnetic resonance (EPR) spectra were obtained on the (Bruker is 5 A300, Germany) paramagnetic resonance spectrometer.

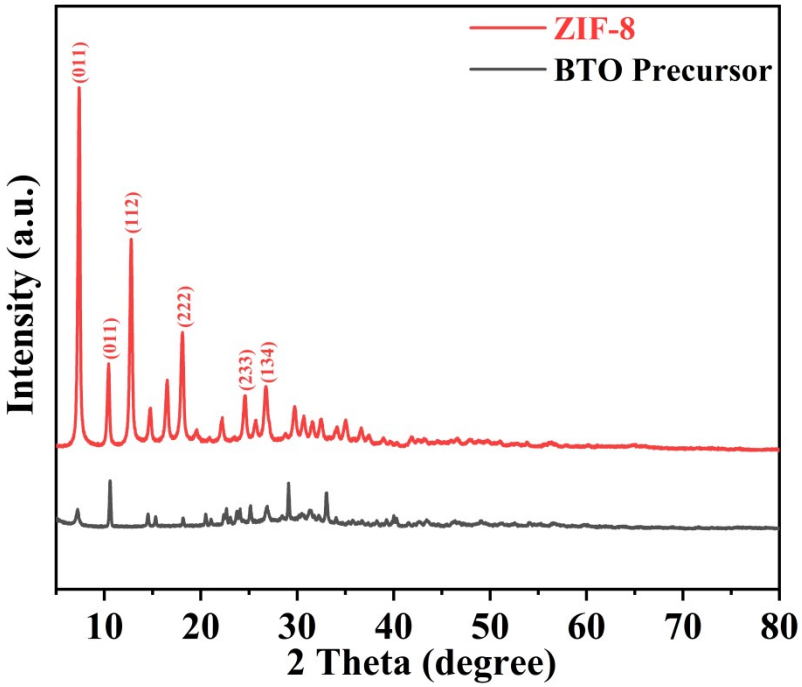


**Fig. S1.** XRD patterns of BTO Precursor and ZIF-8.

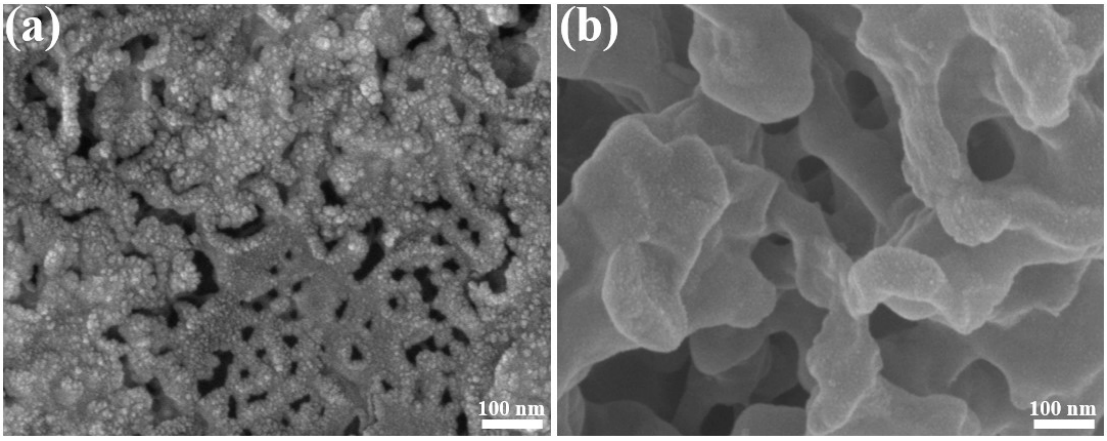


**Fig. S2.** SEM image of: (a) BTO Precursor and (b) ZIF-8.

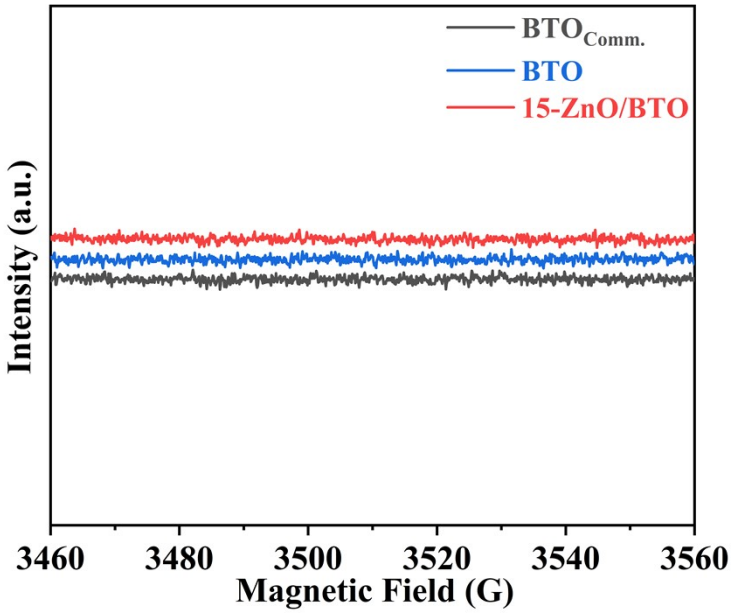


**Fig. S3.** EPR spectra of $BTO_{Comm.}$, BTO and 15-ZnO/BTO: Tiv.

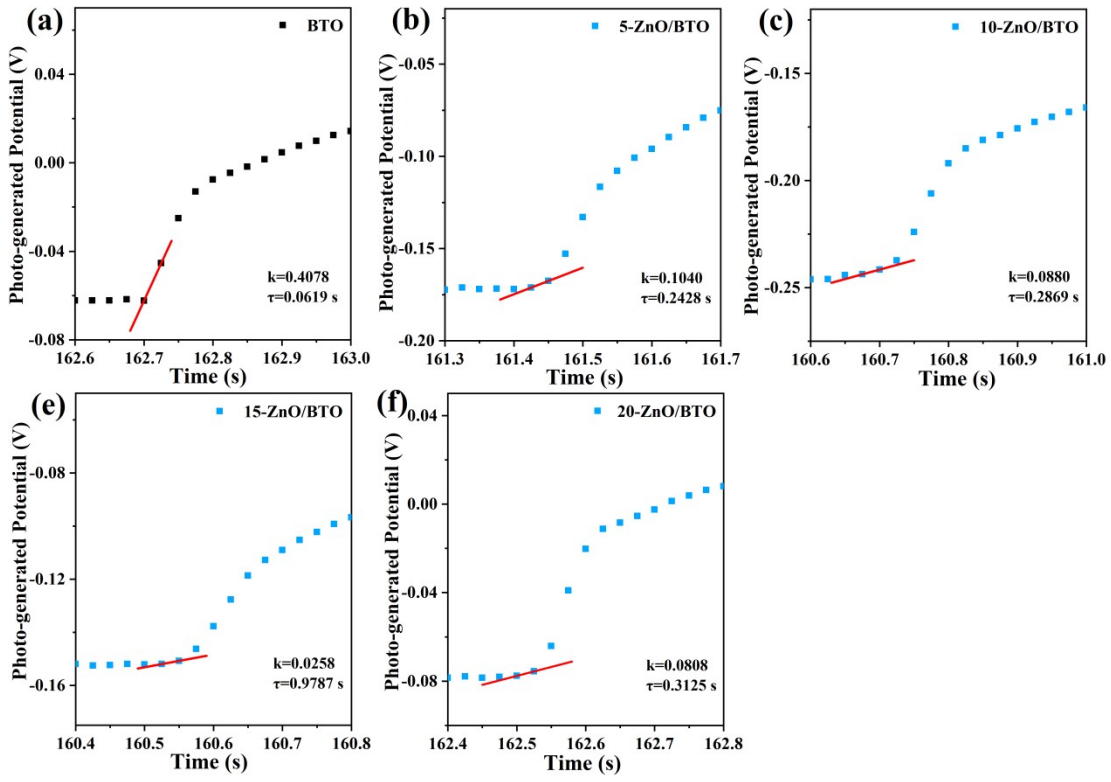


**Fig. S4.** Life-time of (a) BTO, (b)5-ZnO/BTO, (c)10-ZnO/BTO, (d)15-ZnO/BTO and (e)20-ZnO/BTO obtained from OCP curves.

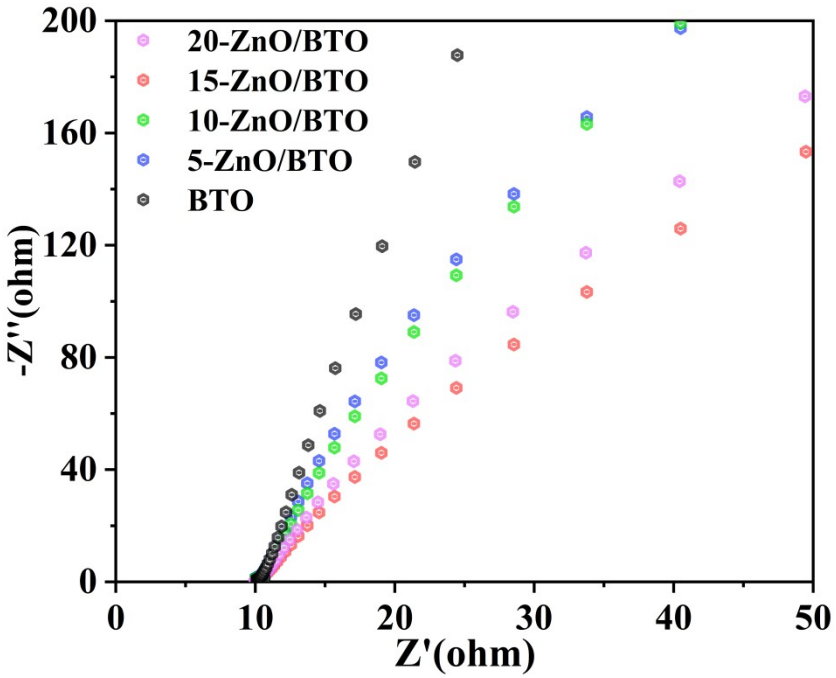


**Fig. S5.** EIS Nyquist plots of BTO, 5-ZnO/BTO, 10-ZnO/BTO, 15-ZnO/BTO and 20-ZnO/BTO.

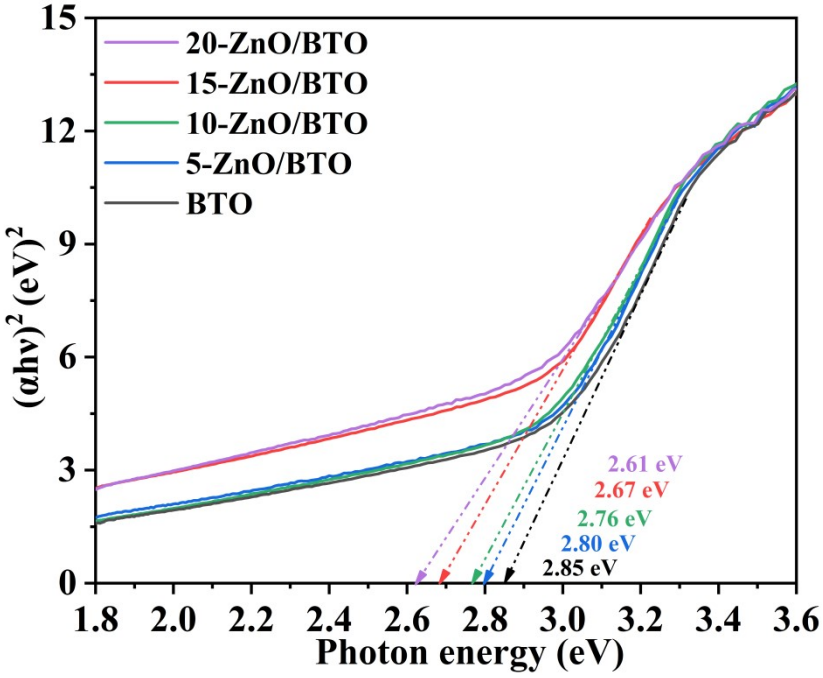


**Fig. S6.** Tauc plots for band gap calculation of BTO, 5-ZnO/BTO, 10-ZnO/BTO, 15-ZnO/BTO and 20-ZnO/BTO.

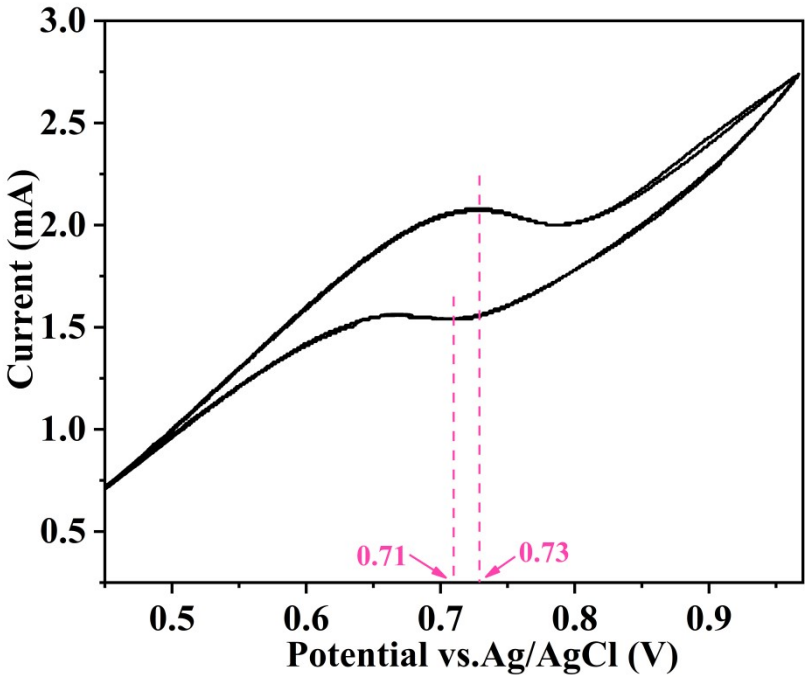


**Fig. S7.** The three-electrode CV curve of redox couple in electrolytes at the scan rate of 50 mV/s.

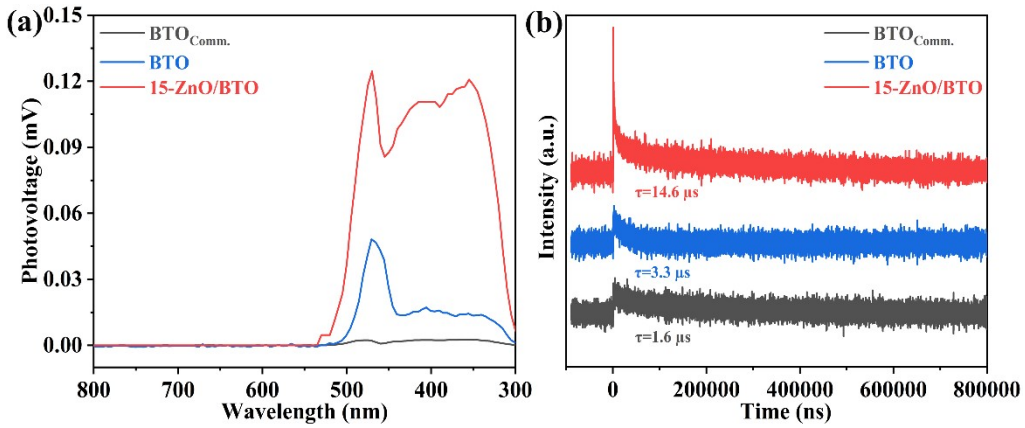


**Fig. S8.** (a) SPV spectroscopy of BTOComm, BTO, and 15- ZnO/BTO; (b) SPV spectroscopy of BTOComm, BTO, and 15- ZnO/BTO.

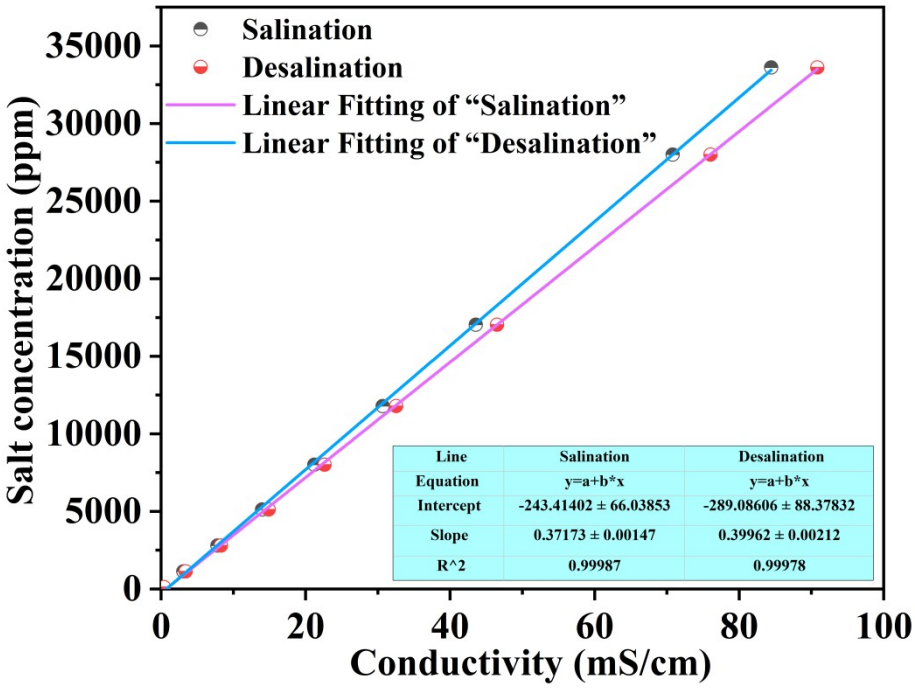


**Fig. S9.** Calibration curve relating NaCl concentration to conductivity.

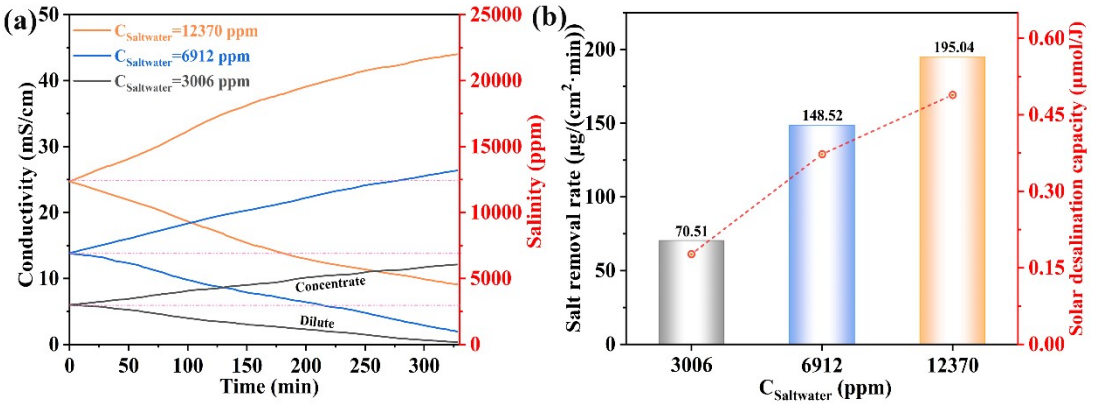


**Fig. S10.** (a) Conductivity Variations and Brine Concentrations During Desalination of Coal Chemical High-Salinity Wastewater with Different Initial Concentrations (3006, 6912, and 12370 ppm); (b) Desalination Performance of Coal Chemical High-Salinity Wastewater with Different Initial Concentrations (3006, 6912, and 12370 ppm).

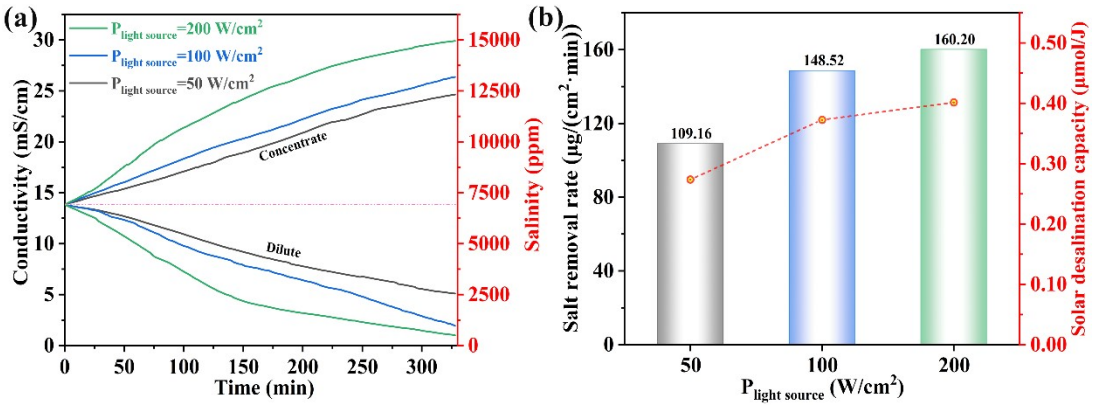


**Fig. S11.** (a) Influence of Different Light Intensities (50, 100, and 200 mW/cm$^2$) on Conductivity Variations and Brine Concentrations During Desalination of Coal Chemical High-Salinity Wastewater; (b) Desalination Performance of Coal Chemical High-Salinity Wastewater Under Different Light Intensities (50, 100, and 200 mW/cm$^2$).

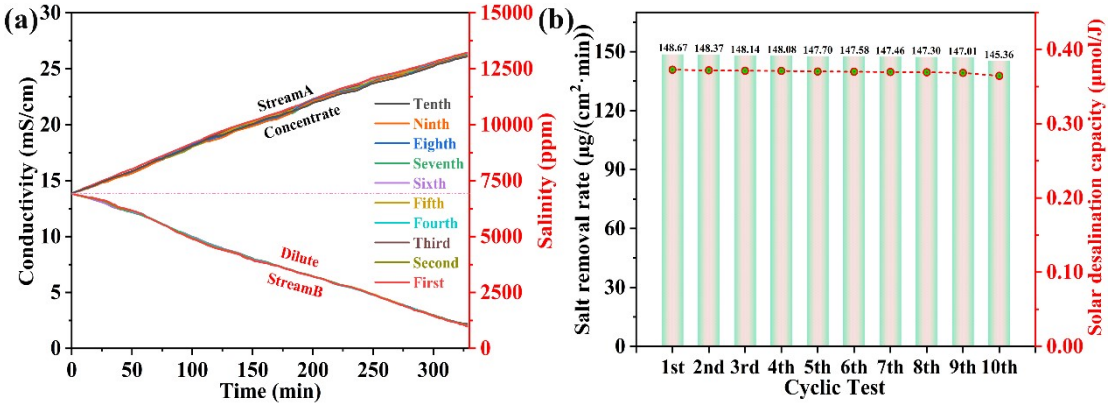


**Fig. S12.** (a) Conductivity changes and salt concentration of the 15-ZnO/BTO photoanode during ten cyclic testing; (b) Desalination performance of the 15-ZnO/BTO photoanode during ten cycling tests.

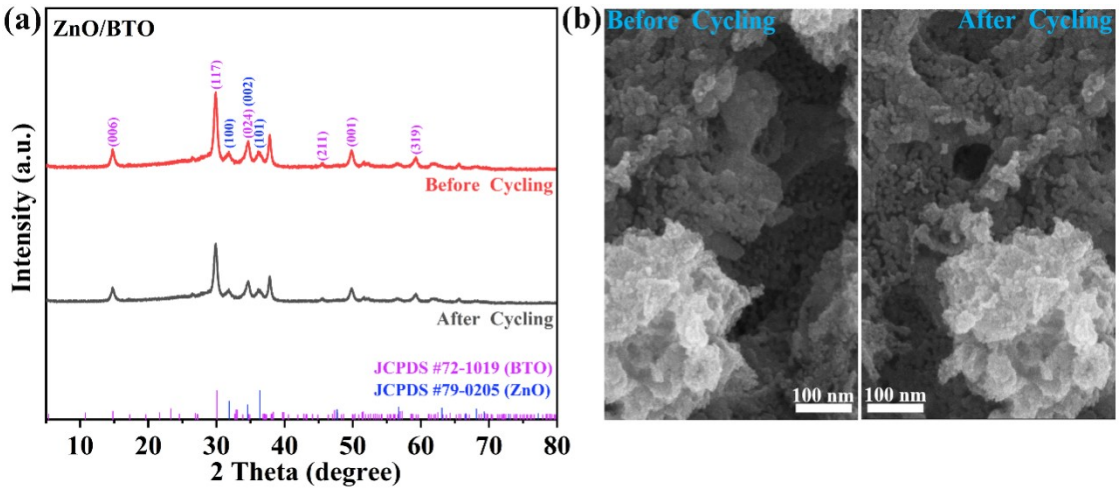


**Fig. S13.** (a)XRD patterns of 15-ZnO/BTO before/after cycling experiment, (b) SEM images of 15-ZnO/BTO before cycling and after cycling.

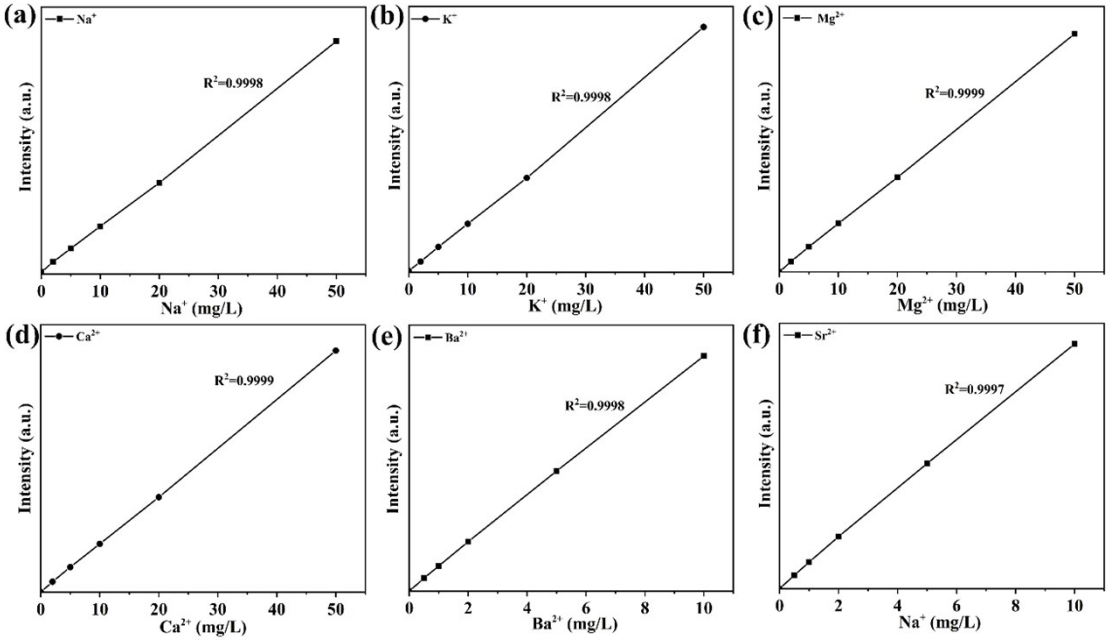


**Fig. S14.** Calibration curves for ion quantification.

.

**Table S1.** List of abbreviation.

| Abbreviation | Full name |
|---|---|
| BTO | $Bi_4Ti_3O_{12}$ |
| SDS | Sodium dodecyl sulfate |
| DMPO | 5,5-dimethyl-1-pyrroline-N-oxide |
| TEMPO | 2,2,6,6-tetramethyl-1-piperidinyloxy |
| CB | conduction band |
| VB | valence band |
| CV | cyclic voltammetry |
| Biv | Bi vacancy |
| Ov | O vacancy |
| PA-ED | Photoanode-Assisted Electrochemical Desalination |
| PEC | Photo-Electro-Chemistry |
| EIS | electrochemical impedance spectroscopy |
| OCP-t | open-circuit voltage experiment |
| SEM | Scanning electron microscopy |
| TEM | Transmission electron microscopy |
| XRD | X-Ray Powder Diffraction |
| XPS | X-ray photoelectron spectroscopy |
| EPR | Electron Paramagnetic Resonance |
| SI-XPS | in-situ irradiation XPS |
| IC | ion chromatography |
| ICP-OES | Inductively coupled plasma optical emission spectrometry |

**Table S2.** Salt removal rates and photocurrent data for BTOComm., BTO and 15-ZnO/BTO photoanodes.

| Electrode | Salt removal rate ($\mu g/(cm^2 \cdot min)$) | Initial photocurrent densities ($mA/cm^2$) | Photocurrent density variation range ($mA/cm^2$) |
|---|---|---|---|
| $BTO_{Comm.}$ | 44.20 | 3.42 | 3.21 |
| BTO | 89.50 | 3.70 | 1.54 |
| 15-ZnO/BTO | 148.52 | 4.65 | 1.25 |

**Table S3.** ICP-OES results of leached ions in different streams after desalination.

| Electrode | BTO | | | 15-ZnO/BTO | | |
|---|---|---|---|---|---|---|
| Item | Redox Electrolyte (mg/L) | Diluted stream (mg/L) | Concentrated stream (mg/L) | Redox Electrolyte (mg/L) | Diluted stream (mg/L) | Concentrated stream (mg/L) |
| $Bi^{3+}$ | 0.0021 | - | 0.0001 | - | - | - |
| $Ti^{4+}$ | 0.0031 | - | 0.0004 | - | - | - |
| $Zn^{2+}$ | / | / | / | - | - | - |

**Table S4.** Initial and final water quality of the high-salinity wastewater treated by SD-PED.

| Item | Unit | Initial | Diluted stream | Removal efficiency |
|---|---|---|---|---|
| Conductivity | mS/cm | 13.96 | 1.66 | 88.10 |
| $Na^+$ | ppm | 3430.95 | 312.00 | 90.91 |
| $Ca^{2+}$ | ppm | 82.94 | 9.06 | 89.07 |
| $K^+$ | ppm | 40.48 | 3.68 | 90.90 |
| $Mg^{2+}$ | ppm | 5.92 | 0.70 | 88.06 |
| $Sr^{2+}$ | ppm | 1.25 | 0.15 | 87.64 |
| $Ba^{2+}$ | ppm | 0.042 | 0.004 | 90.47 |
| $CI^-$ | ppm | 5253.30 | 495.93 | 90.56 |
| $NO_3^-$ | ppm | 247.01 | 23.95 | 90.30 |
| $CO_3^{2-}$ | ppm | - | - | - |
| $SO_4^{2-}$ | ppm | - | - | - |

**Table S5.** Summary of solar desalination performance in this work.

| Electrode | Salt concentration (ppm) | Desalination rate ($\mu g \cdot cm^{-2} \cdot min^{-1}$) | Specific power of the light source ($W/cm^2$) | Solar desalination capacity(μmol/J) |
|---|---|---|---|---|
| $BTO_{Comm.}$ | 6912 | 44.20 | 100 | 0.116 |
| BTO-10 | 6912 | 54.53 | 100 | 0.125 |
| BTO-20 | 6912 | 63.55 | 100 | 0.131 |
| BTO-30 | 6912 | 89.50 | 100 | 0.205 |
| BTO-40 | 6912 | 79.26 | 100 | 0.177 |
| BTO-50 | 6912 | 69.30 | 100 | 0.147 |
| 5-ZnO/BTO | 6912 | 105.93 | 100 | 0.252 |
| 10-ZnO/BTO | 6912 | 124.66 | 100 | 0.306 |
| 15-ZnO/BTO | 6912 | 148.52 | 100 | 0.365 |
| 20-ZnO/BTO | 6912 | 132.05 | 100 | 0.328 |

**Table S6.** Comparison with recent reports on solar-driven photoelectrochemical desalination.

| Electrode | Redox couple | Salt concentration (ppm) | Photocurrent density (mA) | Desalination rate ($\mu g cm^{-2} min^{-1}$) | Specific power of the light source ($W/cm^2$) | Solar desalination capacity (μmol/J) | Publication time | Reference |
|---|---|---|---|---|---|---|---|---|
| ZnO/BTO | $I^-/I^{3-}$ | 6912 | 4.65 | 148.52 | 100 | 0.365 | / | This work |
| $CuBi_2O_4$/NiO | $[Fe(CN)_6]^{3-/4-}$ | 7400 | 1.52 | 54.30 | 200 | 0.077 | 2026 | [1] |
| NiO/$CuInS_2$ | $[Fe(CN)_6]^{3-/4-}$ | 4000 | 1.06 | 11.91 | 106 | 0.032 | 2025 | [2] |
| NiO@$Co_3O_4$/$BiVO_4$ | $I^-/I^{3-}$ | 3230 | 3.01 | 88.76 | 100 | 0.231 | 2025 | [3] |
| $CeO_2$/ $BiVO_4$/$MoO_3$ | $[Fe(CN)_6]^{3-/4-}$ | 5000 | 4.52 | 107.43 | 100 | 0.135 | 2025 | [4] |
| $Co_3O_4$@NC/$BiVO_4$ | $I^-/I_3^-$ | 2013 | 2.40 | 69.01 | 100 | 0.187 | 2025 | [5] |
| $Fe_2O_3$/$BiVO_4$ | $I^-/I_3^-$ | 1350 | 1.92 | 44.62 | 100 | 0.127 | 2024 | [6] |
| $WO_3$/$BiVO_4$ | $I^-/I^{3-}$ | 4000 | 2.93 | 65.03 | 200 | 0.093 | 2023 | [7] |
| FeMn-PBA@MXene | $[Fe(CN)_6]^{3-/4-}$ | 4000 | 1.23 | 27.75 | 200 | 0.006 | 2023 | [8] |
| CdS/$BiVO_4$ | $I^-/I_3^-$ | 4000 | 2.58 | 57.30 | 232 | 0.070 | 2022 | [9] |
| $Bi_2O_3$/N719 | $[Fe(CN)_6]^{3-/4-}$ | 4000 | 2.60 | 43.78 | 153 | 0.210 | 2020 | [10] |

**Table S7.** Economic cost for SD-PED device in this work.

| | Iitem | Unit price | Consumption (This work) | Cost |
|---|---|---|---|---|
| Upfront cost | PTFE capillaries | 0.14 USD·m$^{-1}$ | 50 cm | 0.07 USD |
| | Silicone gaskets | 95 USD/·m$^{-2}$ | 72 cm$^2$ | 0.69 USD |
| | Chamber | / | 4 pieces | 34.0 USD |
| Consumables | Ion exchange membrane (AEM, CEM) | 327 USD/·m$^{-2}$ | 22 cm$^2$ | 0.70 USD |
| | $I^-/I^{3-}$electrolyte | 6.0 USD·L$^{-1}$ | 50 ml | 0.30 USD |
| | Total cost | / | / | 35.5 USD |
| Energy cost | Power consumption (Peristaltic pump) | 0.09 W × 3 | 6.0 h (in 6912 ppm) | 1.62 W·h |
| Energy consumption | | 1.62 W·h | 10 mL | 162.0 kW·h/m$^3$ |
| Water Production Cost | / | 0.093 USD/ kW·h | 1 m$^3$ | 15.0 USD/m$^3$ |
| | Desalination rate | / | 0.48 mL/h | / |

**Table S8.** Comparative assessment of energy efficiency and overall system cost for SD-PED technology versus conventional desalination technologies (electricity cost: 0.093 USD/ kW·h).

| Desalination technology | Energy consumption ($kW \cdot h/m^3$) | Water Production Cost ($USD/m^3$) | Key feature | References |
|---|---|---|---|---|
| SD-PED | 162.0 | 15.0 | Photovoltaic-driven | This Work |
| RO | 2.91-6.0 | 0.45-1.72 | Electric-driven | [11] |
| ED | ~4.11 | ~0.55 | Electric-driven | [11, 12] |
| MED | ~25.0 | ~1.28 | Thermal-driven | [13] |
| MSF | 23.1-25.5 | 0.96 - 2.83 | Thermal-driven | [12, 13] |

# References


1. S. Yuan, M. Luo, W. Zhou, J. Li, Y. Cao, K. S. Hui, Y. Yang, Y. Wang, X. Li, Y. Yang, F. Chen, Ammonium ion-assisted electrodeposition of $CuBi_2O_4$/NiO photocathodes for efficient photoelectrochemical desalination, *Desalination*, 2026, **627**,120023.
2. X. Wang, Y. Wang, X. Chen, L. Liu, K. S. Hui, L. Guo, M. Luo and F. Chen, Photocathode-assisted desalination device based on NiO/$CuInS_2$ heterostructure, *Journal of Environmental Chemical Engineering*, 2025, **13** (5), 117925.
3. J. Li, M. Luo, S. Yuan, X. Hai, Y. Zhao, F. Chen, J. Han, X. Li and Y. Yang, In-situ engineered Ni-Co bimetallic hole transport layers for enhanced photoelectrochemical desalination performance, *Desalination*, 2025, **613**, 119106.
4. S. Yuan, M. Luo, Y. Cao, J. Li, X. Wu, J. Han, Y. Yang, X. Li and F. Chen, Three-phase heterostructure photoanode of $CeO_2$/$BiVO_4$/$MoO_3$ for enhanced photo-electrochemical desalination, *Chemical Engineering Journal*, 2025, **515**, 163436.
5. J. Li, S. Yuan, X. Zhang, F. Chen, Y. Yang, J. Kang, Y. He, J. Han, X. Li, Y.Yang and M. Luo, Enhanced photoelectric desalination of $Co_3O_4$@NC/$BiVO_4$ photoanode via in-situ construction of hole transport layer, *Journal of Colloid and Interface Science*, 2025, **680**, 11-23.
6. S. Yuan, W. Ding, J. Li, X. Wang, Y. Zhang, Y. Zhao, F. Chen, X. Li and M. Luo, Design and Construction of the $Fe_2O_3$/$BiVO_4$ Heterostructure-Based Photoanode for Photo-Electrochemical Desalination, *ACS Sustainable Chemistry & Engineering*, 2024, **12** (16), 6330-6342.
7. J. Zhang, Y. Zi, W. Shan, P. Songsiriritthigul, M. Luo, T. Z. Oo, M. Zaw, N. W. Lwin, S. H. Aung, G. Ying and F. Chen, The solar-driven redox seawater desalination based on the stable and environmentally friendly $WO_3$/$BiVO_4$ photoanode, *Desalination*, 2023, **566**, 116939.
8. H. Hu, H. Lin, X. Chen, Y. Pan, X. Li, Z. Zhuang, H. Chen, X. Wang, M. Luo, K. Zheng, L. Zhang and F. Chen, Fe, Mn-Prussian blue analogue@MXene composites for efficient photocatalytic peroxydisulfate-activated degradation of tetracycline hydrochloride and photoelectrochemical desalination, *Chemical Engineering Journal*, 2023, **476**, 146682.
9. M. liang, J. Zhang, K. Ramalingam, Q. Wei, K. San Hui, S. Htike Aung, K. Nam Hui and F. Chen, Stable and efficient self-sustained photoelectrochemical desalination based on CdS QDs/$BiVO_4$ heterostructure, *Chemical Engineering Journal*, 2022, **429**, 132168.
10. J. Zhang, X. Wang, M. Liang, M. Han, J. Dai, Q. Wei, T. Z. Oo, S. H. Aung, K. N. Hui and F. Chen, High-Performance Photoelectrochemical Desalination Based on the Dye-Sensitized $Bi_2O_3$ Anode, *ACS Applied Materials & Interfaces*, 2022, **14** (29), 33024-33031.
11. C. El Younossi, A. El Fadar, Y. Elaouzy, Comprehensive investigation of desalination technologies considering numerous plants worldwide, *Applied Thermal Engineering*, 2025, **278**,127216.

12. Q. N. Al-Oweiti, O. G. Kaoud, M. H. Elbassoussi, S. M. Zubair, Techno-economic evaluation of hybrid multi-effect and membrane desalination systems for improved water production, *Energy Conversion and Management*, 2026, **347**,120548.
13. B. Benhala, F. Loirdighi, A. Assir, M. El Khaili, H. Nhaila, A. Raihani, M. Qbadou, A. Sallem, Comparative Analysis of Desalination Technologies: Energy Performance and Renewable Energy Integration with Focus on Reverse Osmosis Systems, *E3S Web of Conferences*, 2025, **680,** 00031.